Since January 2020 Elsevier has created a COVID-19 resource centre with free information in English and Mandarin on the novel coronavirus COVID-19. The COVID-19 resource centre is hosted on Elsevier Connect, the company's public news and information website.

Antiviral Research 204 (2022) 105365

Contents lists available at ScienceDirect

Antiviral Research

journal homepage: www.elsevier.com/locate/antiviral

Bergamottin, a bioactive component of bergamot, inhibits SARS-CoV-2 infection in golden Syrian hamsters

Minmin Zhou [a,b], Yang Liu [a], Junyuan Cao [a,b], Siqi Dong [a,b], Yuxia Hou [a,b], Yan Yu [c,d], Qiuyan Zhang [a], Yueli Zhang [a,e], Xiaoying Jia [a,b], Bo Zhang [a,b], Gengfu Xiao [a,b], Gang Li [c], Wei Wang [a,b,*]

[a] State Key Laboratory of Virology, Wuhan Institute of Virology, Center for Biosafety Mega-Science, Chinese Academy of Sciences, Wuhan, 430071, China
[b] University of the Chinese Academy of Sciences, Beijing, 100049, China
[c] Nanfang Hospital, Southern Medical University, Guangzhou, 510515, China
[d] Guangdong Engineering and Technology Research Centre of Organoid, Guangzhou, 510515, China
[e] College of Pharmacy and State Key Laboratory of Medicinal Chemical Biology, Nankai University, Tianjin, 300450, China

ARTICLE INFO

Keywords:
SARS-CoV-2
Natural products
Antiviral
Inhibitor
Bergamottin

ABSTRACT

Severe acute respiratory syndrome coronavirus-2 (SARS-CoV-2) has caused an ongoing pandemic, coronavirus disease-2019 (COVID-19), which has become a major global public health event. Antiviral compounds remain the predominant means of treating COVID-19. Here, we reported that bergamottin, a furanocoumarin originally found in bergamot, exhibited inhibitory activity against SARS-CoV-2 *in vitro, ex vivo,* and *in vivo*. Bergamottin interfered with multiple stages of virus life cycles, specifically blocking the SARS-CoV-2 spike-mediated membrane fusion and effectively reducing viral RNA synthesis. Oral delivery of bergamottin to golden Syrian hamsters at dosages of both 50 mg/kg and 75 mg/kg reduced the SARS-CoV-2 load in nasal turbinates and lung tissues. Pathological damage caused by viral infection was also ameliorated after bergamottin treatment. Overall, our study provides evidence of bergamottin as a promising natural compound, with broad-spectrum anti-coronavirus activity, that could be further developed in the fight against COVID-19 infection during the current pandemic.

1. Introduction

Up to May 2022, 511,965,711 confirmed cases of COVID-19 had been reported globally, including 6,240,619 deaths, according to the World Health Organization (WHO). So far, a total of five new coronavirus variants have been identified as "variants of concern" by the WHO, namely Alpha (B.1.1.7), Beta (B.1.351), Gamma (P.1), Delta (B.1.617.2), and the latest, Omicron (B.1.1.529). The emerging variants and mutations of SARS-CoV-2 have posed a great challenge to public health and safety.

SARS-CoV-2 combines high infectivity with serious pathogenicity, which belongs to the same lineage B *Beta coronavirus* (Hu et al., 2021). SARS-CoV-2 is an enveloped, single-stranded positive-stranded RNA virus with genomes encoding four structural proteins: envelope protein (E), matrix glycoprotein (M), nucleocapsid protein (N), and spike protein (S). The S protein is a class I membrane fusion protein (Zhu et al., 2020), where the S1 subunit is responsible for angiotensin-converting enzyme 2 (ACE2) recognition, and the S2 subunit is involved in membrane fusion (Lan et al., 2020), which plays a key role in the entry process of the virus into a host cell. Infection is triggered by viral binding to the cell surface receptor ACE2 (Benton et al., 2020; Zhou et al., 2020), followed by a spike-mediated cell membrane fusion, releasing the viral genome into the host cell. During replication, viral replicase polyprotein is processed by the chymotrypsin-like cysteine protease ($3CL^{pro}$) and papain-like protease (PL^{pro}) to form a functional viral replication complex (V'Kovski et al., 2021).

Vaccination is the critical solution for COVID-19 prevention and pandemic control (Awadasseid et al., 2021). To date, 151 candidate vaccines are undergoing preclinical evaluation. Given the discrepancies in popularity, the speed of vaccination, and the distribution of vaccines varies around the world, the epidemic situation is very different between regions, countries, provinces, and towns. Meanwhile, in the context of

* Corresponding author. State Key Laboratory of Virology, Wuhan Institute of Virology, Center for Biosafety Mega-Science, Chinese Academy of Sciences, Wuhan, 430071, China.
E-mail address: wangwei@wh.iov.cn (W. Wang).

https://doi.org/10.1016/j.antiviral.2022.105365
Received 18 March 2022; Received in revised form 13 June 2022; Accepted 13 June 2022
Available online 19 June 2022

the global spread of SARS-CoV-2, the virus has adapted to the host stepwise. Aside from vaccines, antiviral drugs are also used against COVID-19, there is still an urgent need for additional safe and effective drugs to combat SARS-CoV-2.

Botanicals and other purified natural products have served as a leading source for novel antiviral drug discovery (Lin et al., 2014). Including the antiviral activities against some vital viral pathogens including coronavirus (CoV) (Cao et al., 2022; Vijgen et al., 2005), dengue virus (DENV) (Lin et al., 2013; Zandi et al., 2012), enterovirus 71 (EV71) (Choi et al., 2009) for example. Based on our previous study, we identified bergamottin as Lassa virus (LASV) entry inhibitor in a micromolar range through high-throughput screening of a botanical drug library and found that bergamottin inhibits LASV entry through blocking LASV endocytic trafficking(Liu et al., 2021). Therefore, we explored the antiviral effect of the natural furanocoumarin, bergamottin, against SARS-CoV-2 infection both *in vitro* and *in vivo*.

2. Materials and methods

2.1. Cells and virus

Human colon Caco-2 cells (ATCC Number: HTB-37), human embryonic kidney HEK-293T cells (ATCC Number: CRL-3216), African green monkey kidney Vero E6 cells (ATCC Number: CRL-1586), baby hamster kidney (BHK-21) cells (ATCC Number: CCL-10), human rhabdomyosarcoma RD cells (ATCC Number:CCL-136), human hepatoma HuH-7 cells (from Microorganisms & Viruses Culture Collection Center, Wuhan Institute of Virology, Chinese Academy of Sciences, Number: IVCAS 9.005) were cultured in Dulbecco's Modified Eagle's Medium (DMEM; HyClone, Logan, UT, USA) and supplemented with 10% fetal bovine serum (GIBCO, Grand Island, NY, USA) at 37 °C and 5% CO_2. All the cell lines were tested negative for mycoplasma contamination.

SARS-CoV-2 strains 2019-nCoV-WIV04, B.1.1.7, and B.1.351 were obtained from the National Virus Resource Center and propagated in Vero E6 cells. All the authentic SARS-CoV-2 infection experiments were carried out at the Biosafety Level 3 facility of Wuhan Institute of Virology, Chinese Academy of Sciences.

2.2. Inhibitors

Bergamottin (HY-N2194) was purchased from MedChemExpress and Weikeqi Biotech (wkq21050802), and it was dissolved in DMSO. The purity of bergamottin obtained from both companies was identified by HPLC as greater than 98%.

Clofazimine (HY-B1046) and Remdesivir (HY-104077) were purchased from MedChemExpress.

2.3. Cell isolation and organoids formation from human nasal polyps

Human nasal polyp tissues were obtained from resections performed at the southern hospital of southern medical university. All patients provided informed consent. Samples were procured and the study was conducted under Institutional Review Board approval before tissue acquisition.

The tissue samples were minced and incubated with digestion buffer consisting of advanced DMEM/F12 supplemented with 0.125 mg/mL dispase II (Wako, Richmond, VA, USA), 0.1 mg/mL DNaseI (MilliporeSigma, Burlington, MA, USA), 0.125 mg/ml collagenase III (Gibco, Carlsbad, CA, USA), 10% Fetal Bovine Serum (Gibco, Australia) and 1% penicillin-streptomycin at 37 °C for 1 h on the shaker. Subsequently, supernatants were filtered through the 100 μm cell strainer (JET BIOFIL, Guangzhou, China), and the suspension was collected by centrifugation at 200*g* for 5 min. The pellets were resuspended in the culture media and mixed with Matrigel (Corning, Corning, NY, USA). The cell-matrigel mix was seeded in a 24-well plate and incubated with an Accurate organoids' expansion medium at 37 °C and 5% CO_2. The culture medium was changed every two to three days.

2.4. Optimized human nasal epithelial organoids differentiation

For differentiation, human nasal epithelial organoid colonies were detached from the culture dish using TrypLE (Gibco). After dissociation, human nasal epithelial organoids were collected as a single cell suspension in a differentiation medium (Expansion Medium containing 0.1 mM IBMX, 0.1 mM 8-Bromo-cAMP, and 60 nM dexamethasone). Cell concentration was determined by an automated cell counter (Countess™ II Automated Cell Counter; Countess II, Life Technologies). The appropriate number of live cells needed for the succeeding experiment was transferred into the differentiation medium, and these organoids were incubated at 37 °C and 5% CO_2 for 14 d. On day 5, half of the spent medium was refreshed.

2.5. Antiviral activity assay and drug cytotoxicity assay

For the antiviral assay, the cell density of seeded Caco-2 cells was 2.5×10^5 cells/ml per well in 96-well plates and grown at 37 °C with 5% CO_2 for 16 h. After pretreatment with the gradient diluted bergamottin for 1 h, cells were infected with SARS-CoV-2 at an multiplicity of infection (MOI) of 0.5 for 1 h in the presence of drugs. After incubation, the inoculum was removed, and culture vessels were refreshed with a drug-containing medium and further maintained until 24 h post-infection. The antiviral activity of bergamottin was measured by immunofluorescence staining assay (IFA). The antibodies used were as follows: primary antibody anti-SARS-CoV-2 NP rabbit antiserum (GeneTex; GTX635678; dilution 1:1000), and secondary antibody DyLightTM 488-labeled goat anti-rabbit IgG (KPL; 5230-0385; dilution 1:1000). The nuclei were counterstained with DAPI.

Concerning the antiviral effect of hCoV-OC43 and hCoV-229E, RD cells and Huh-7 cells were seeded at 2.0×10^5 cells/ml per well in 12-well plates and grown at 37 °C with 5% CO_2 for 16 h. After pretreatment with the gradient diluted bergamottin for 1 h, cells were infected with SARS-CoV-2 at an MOI of 0.1 for 1 h in the presence of drugs. After incubation, the inoculum was removed, and culture vessels were refreshed with a drug-containing medium and further maintained until 24 h post-infection. Total cell RNA was extracted and the antiviral activity of bergamottin was measured using RT-qPCR.

Human nasal epithelial organoids were seeded in 96-well plates, and it was pre-treated with the indicated concentration of bergamottin or 10 μM remdesivir as a positive control for 1 h before infection. Organoids were infected with SARS-CoV-2 at an MOI of 1 in the presence of drugs, total cell RNA was extracted to evaluate the virus infectivity after 24 h post-infection.

For drug cytotoxicity assays, Caco-2 cells were seeded in 96-well plates at a density of 2.5×10^5 cells/ml, RD and Huh-7 cells were seeded in 96-well plates at a density of 2.0×10^5 cells/ml. Appropriate concentrations of bergamottin were added to the medium 16 h later. After 24 h incubation, the relative number of surviving cells was measured using the Cell Counting Kit 8 (CCK-8) assay (Beyotime, China), followed by the manufacturer's instructions. Absorbance was measured at 450 nm wavelength.

2.6. RT-qPCR

Total cell RNA was extracted using TRIzol reagent. Reverse transcription was performed by HiScript II Q RT SuperMix (Vazyme Biotech, Nanjing, China) and a random hexamer. Viral RNA detection was performed using RT-qPCR.

SARS-CoV-2 RBD Forward: 5′_CAATGGTTTAACAGGCACAGG_3′

SARS-CoV-2 RBD Reverse: 5′_CTCAAGTGTCTGTGGATCACG_3′

HCoV-229E M protein Forward: 5′_TTCCGACGTGCTCGAACTTT_3′

HCoV-229E M protein Reverse: 5′_CCAACACGGTTGTGACAGTGA_3′

HCoV-OC43 M protein Forward: 5′_ ATGTTAGGCCGATAATTGA GGACTAT_3′

HCoV-OC43 M protein Reverse: 5′_ AATGTAAAGATGGCCGCGTA TT_3′

2.7. Spike-mediated membrane fusion assay

Vero E6 cells were transfected with 0.25 μg SARS-CoV-2 S ct19 plasmid and 0.25 μg EGFP plasmid simultaneously, the cell medium was replaced with 2% DMEM supplemented with different concentrations of compounds 4 h post-transfection. Syncytium formation was observed 16–24 h later, and images were captured using an M-shot image analysis system (Micro-shot Technology, Guangzhou, China).

2.8. A dual-split-protein (DSP)-based cell-cell fusion assay

Briefly(Zhu et al., 2020), a total of 4×10^5 cells/ml of 293T cells were seeded in 96-well (effector cells) and 6-well plates (target cells) respectively. On the next day, 293T cells seeded in the 96-well were transfected with an S protein-expressing plasmid and a DSP_{1-7} plasmid, whereas the 293T cells seeded in the 6-well were transfected with a DSP_{8-11} plasmid. After 24 h post transfection, gradient diluted bergamottin was added to the effector cells and incubated for 1 h. Meanwhile, the target cells were resuspended at a density of 3×10^5 cells/ml in prewarmed 2% DMEM containing EnduRen live-cell substrate (Promega Corporation, Madison, WI, USA), the final concentration of which is 0.35 mg/ml. Diluted target cells were transferred to the effector cells as indicated. The mixture containing two kinds of the cells was spun down to maximize cell-cell contact; next, the changes of luciferase activity was measured after a 24 h incubation, and representative images were captured.

2.9. Time-of-addition assay

Caco-2 cells were infected with SARS-CoV-2 for 1 h. Bergamottin (35 μM) was incubated with the cells for 1 h or 8 h according to the following conditions: pre-infection (−1 to 0 h), during infection (0–1 h), and post-infection (1–8 h).

To evaluate the virucidal effect of bergamottin, it was first incubated directly with SARS-CoV-2 at 37 °C for 1 h, and then the drug-virus mixture was 25 times diluted to infect cells (MOI = 0.5). The infectivity of the remained viruses was determined using IFA.

2.10. Viral RNA replicon assay

The SARS-CoV-2 replicon was constructed as previously described (Zhang et al., 2021). Briefly, BHK-21 cells were electroporated with SARS-CoV-2 replicon, and then cells were treated with the indicated concentration of bergamottin or 10 μM remdesivir as control. A mutant replicon-ΔRdRp with a 339–934 amino acid deletion within the RNA-dependent RNA polymerase (RdRP) also known as nsp12 was performed as a negative control (data not shown). Luciferase activity was measured after 24 h.

2.11. Effect on $3CL^{pro}$ protease activity

All assays were performed in 50 mM HEPES (pH 7.0) and 2 mmol/L DTT. The experiment was initiated by adding SARS-CoV-2 $3CL^{pro}$ to different concentrations of substrate (10–200 μM). The absorbance value was monitored. Different concentrations of bergamottin were added to the enzymatic reaction mixture, the reduction of the values was calculated to evaluate the inhibitory effect.

2.12. Effect on the binding between SARS-CoV-2 RBD and ACE2

The SARS-CoV-2 (2019-nCoV) Inhibitor Screening ELISA Kit (Sino-Biological, Cat# KIT001) was used to determine the effect of bergamottin on the binding between SARS-CoV-2 RBD and ACE2. Gradient diluted compounds or DMSO were added to compete with ACE2-His (Cat: 10108-H08B) to combine with immobilized SARS-CoV-2 S Protein RBD. The absorbance at 450 nm was measured.

2.13. Effect on the expression of ACE2 and TMPRSS2

Caco-2 cells were incubated with the indicated concentration of bergamottin for 20 h, and cell lysates were collected in the cell lysis buffer (Beyotime, Shanghai, China). Proteins were separated by sodium dodecyl sulfate (SDS) polyacrylamide gel electrophoresis. The antibodies used were as follows: primary antibody human ACE2 Rabbit mAb (ABclonal; A4612; dilution 1:1000), humanTMPRSS2 Rabbit mAb (ABclonal; A9126; dilution 1:1000).

2.14. SARS-CoV-2 challenge and inhibitor administration in the golden Syrian hamster model

All animal experiments conformed to the standards for use and care of laboratory animals and were approved by the Institutional Review Board of the Wuhan Institute of Virology, Chinese Academy of Sciences.

Adult male Syrian hamsters (6–8 weeks old) were obtained from Beijing Vital River Laboratory Animal Technology and raised at pathogen-free animal feeding facilities. The animal experiments were conformed to the use and care of laboratory animals and were approved by the Institutional Review Board of the Wuhan Institute of Virology, CAS. Hamsters were randomly assigned to six groups: three of these groups were tested for drug toxicity by gavage with different doses of bergamottin and corn oil for 5 consecutive days, body weights of hamsters were monitored every day. Whereas the remaining three groups were infected with SARS-CoV-2 and then underwent vehicle or bergamottin treatment. For infection, each hamster was intranasally inoculated with 5×10^4 PFU SARS-CoV-2 strain 2019-nCoV-WIV04 at 0 dpi. Following infection, one group (control) received only the vehicle (corn oil), whereas the two remaining groups received bergamottin (either 50 mg/kg or 75 mg/kg body weight per hamster). Corn oil was used as the vehicle. Bergamottin or vehicle treatment was administered orally once a day from 0 until 4 dpi. Body weights and symptoms were monitored daily.

Hamsters were sacrificed at 4 dpi for virological and histopathological analyses. Nasal turbinates and lung samples were collected and ground with 1 ml DMEM. Following centrifugation, the supernatant containing virus particles was collected and serially diluted tenfold prior to infecting Vero-E6 cells. Viral titers were assessed per gram of tissues by plaque assay. Meanwhile, the viral yield in harvested hamster tissues was determined using RT-qPCR. Briefly, RNA was purified using the RNeasy Mini Kit (Qiagen). The viral burden was calculated using a standard curve produced using serial tenfold dilutions of plasmids carrying the SARS-CoV-2 spike.

2.15. Hematoxylin and eosin (H&E) staining

For histopathological analysis, lung tissues were harvested from

hamsters and fixed in 4% paraformaldehyde for paraffin embedding. The standard H&E staining protocol was followed for tissue staining, and the changes in lung tissues were observed under a light microscope.

2.16. Statistical analysis

Statistical analysis was performed using GraphPad Prism 8 software (GraphPad Inc., La Jolla, CA, USA). Survival data were analyzed using the log-rank test, and all other statistical analyses were assessed with the student's t-test. P values < 0.05 were considered significant. Data are shown as mean ± standard error.

3. Results

3.1. Antiviral effect of bergamottin on SARS-CoV-2 and emerging variants

To evaluate the antiviral efficacy of bergamottin, IFA was performed to detect virus infection activity. SARS-CoV-2 nuclear protein (NP) was stained to mark the infected cells. Bergamottin exhibited a dose-dependent inhibitory effect on SARS-CoV-2 infection (Fig. 1A). We determined that bergamottin had a half-maximal inhibitory concentration (IC_{50}) of 9.64 μM against SARS-CoV-2. We also tested the antiviral effect of bergamottin on some emerging SARS-CoV-2 variants and obtained IC_{50} values of 8.15 μM and 14.16 μM against B.1.1.7 (Alpha) and B.1.351 (Beta), respectively. The 50% cytotoxic concentration (CC_{50}) of bergamottin on Caco-2 cells was >100 μM, and the selective index (SI; CC_{50}/IC_{50}) for SARS-CoV-2 was >10. (Fig. 1B)

3.2. Bergamottin interferes with various steps of SARS-CoV-2 life cycles

To explore the mechanism underlying the antiviral effect, a time-of-drug-addition assay was carried out to investigate which stage bergamottin worked. To evaluate the virucidal effect of bergamottin, it was firstly incubated with SARS-CoV-2 (2×10^6 PFU/mL) at 37 °C for 1h. Thereafter, the mixture containing bergamottin and the virus was diluted 25 times to infect cells at an MOI of 0.5. The residual infectivity was tested and bergamottin slightly, but directly inactivated SARS-CoV-2. We then tested whether bergamottin acted on the corresponding infection process by varying the time of drug additions, with bergamottin treatment at -1h, 0h, or 1h relative to infection. Bergamottin displayed an inhibitory effect when it was added at 1h before infection; however, when added at the same time as the infection or 1h after infection, bergamottin exhibited stronger inhibitory effects (Fig. 2A).

Next, a VSV-based SARS-CoV-2 S protein-bearing pseudovirus (pv) (Cao et al., 2022) was used to assess the efficacy of bergamottin on virus entry (Fig. 2B). Bergamottin showed a dose-dependent inhibition of SARS-CoV-2 pv infection with an IC_{50} of 48.83 μM. Notably, it was found that bergamottin inhibited SARS-CoV-2 spike-mediated membrane fusion, and the fusion was completely blocked when treated with bergamottin at 25 μM (Fig. 2C). Dual-split-protein (DSP) based cell fusion assay was carried out to quantitatively evaluate the effect of bergamottin on membrane fusion efficiency. Consistent with the observed fluorescent microscopy images captured, bergamottin dose-dependently inhibited spike-mediated membrane fusion activity (Fig. 2D). Since receptor binding acted as the upstream scene of membrane fusion(Acciani et al., 2017; Yu et al., 2022), and the inhibition on receptor binding or expression would lead to a decrease in membrane fusion, we further tested the effects of bergamottin on receptor binding and expression. As shown in Fig. 2E and F, bergamottin showed little effect on the receptor binding domain (RBD), while it inhibited the cellular ACE2 expression in a dose-dependent manner and exerted a moderate inhibition on transmembrane protease serine 2 (TMPRSS2) expression with the highest tested concentration.

We further confirmed the impact of bergamottin on viral replication and post-entry step of infection. Replicon transfected cells were incubated with bergamottin and changes in luciferase activity were detected at 24 h post-transfection (Fig. 2G). Bergamottin showed inhibitory effects on SARS-CoV-2 RNA synthesis. We further tested the effects of bergamottin on SARS-CoV-2 $3CL^{pro}$ protease activity. As shown in Fig. 2H, bergamottin treatment had little effect on protease activity (Fig. 2H).

3.3. Broad-spectrum anti-coronavirus activity of bergamottin

To test whether bergamottin could extend its antiviral effect to other coronaviruses, human pathogenic coronaviruses, hCoV-OC43, and hCoV-229E, were utilized. The robust antiviral effects of bergamottin against both viruses were observed. Bergamottin inhibited hCoV-OC43 infection in RD cells and hCoV-229E infection in Huh-7 cells with the IC_{50} values of 0.274 μM and 5.687 μM, respectively (Fig. 3). The CC_{50} values of bergamottin on Huh-7 and RD cells were >100 μM. The SI values were >17 for hCoV-229E and >364 for hCoV-229E, respectively, indicating that bergamottin has broad-spectrum anti-coronavirus activity. Bergamottin exhibited diverse antiviral effects, with an IC_{50} ranging from 0.274 μM to 14.16 μM, within the micromolar magnitude in general, which may have been due to the following factors: (1) the varied MOI: Caco-2 cells were infected with SARS-CoV-2 at an MOI of 0.5 whereas RD and Huh-7 cells were infected with hCoV-229E and hCoV-OC43 at an MOI of 0.1, and (2) the different detection methods: RT-qPCR was employed to detect hCoV-229E and hCoV-OC43 viral RNA, whereas IFA was used to assess the antiviral effects of SARS-CoV-2.

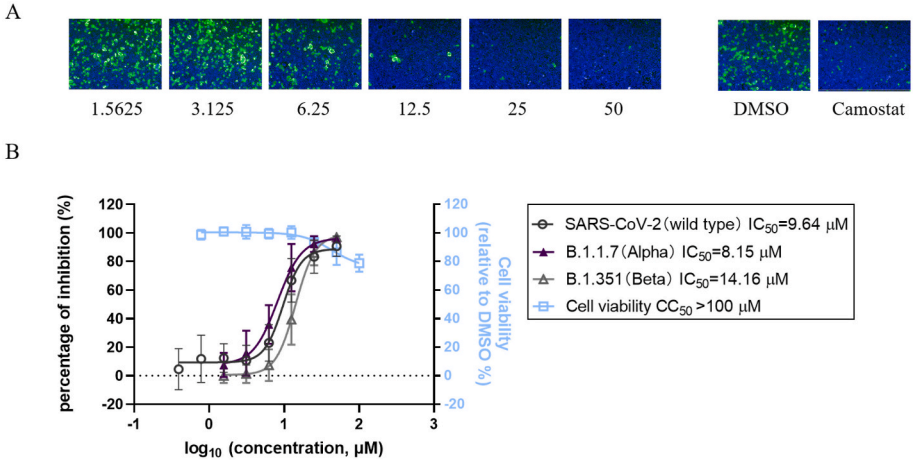

Fig. 1. Effect of bergamottin on SARS-CoV-2 infection. (A) The antiviral effects of bergamottin against SARS-CoV-2 in Caco-2 cells. IFA assay showing the SARS-CoV-2 NP (green) and nuclei (blue) were displayed. 50 μM camostat was used as positive control. (B) Dose-response curves and table of IC_{50} values of bergamottin for inhibition of SARS-CoV-2 and SARS-CoV-2 variants (B.1.1.7 and B.1.351). Drug cytotoxicity was determined by CCK-8 assay. Data represents mean ± SD for n = 3 biological replicates.

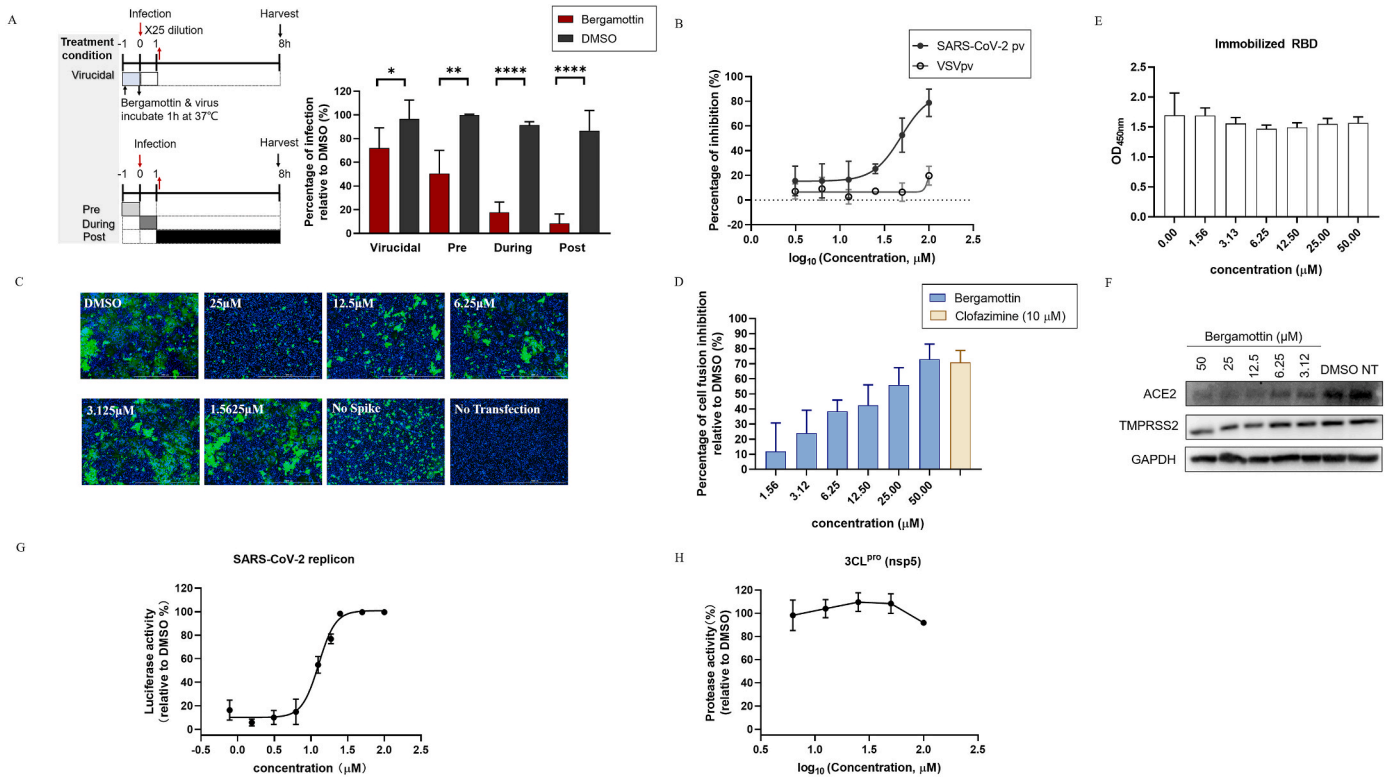

Fig. 2. Effect of Bergamottin on SARS-CoV-2 life cycles. (A) Time-of-addition assay. SARS-CoV-2 infected Caco-2 cells were incubated with bergamottin at indicated time points as the diagram shows. Infection at 8h post-infection was quantified by immunostaining for NP. Data represents mean ± SD for n = 3 biological replicates. (B) Bergamottin inhibited VSV-based SARS-CoV-2 pv infection. Caco-2 cells were pretreated with the indicated concentration of bergamottin and infected with a pseudovirus. Luciferase activity was measured 24 h later. (C) Bergamottin inhibited SARS-CoV-2 S protein-mediated membrane fusion. Vero E6 cells co-transfected with SARS-CoV-2 spike and EGFP plasmids. After 4 h post-transfection, the medium was replaced by bergamottin and the images were acquired 24 h later using fluorescent microcopy. Scale bar: 1000 μm. Representative images selected from three independent experiments are shown. (D) Dual-split-protein (DSP)-based cell-cell fusion assay. The effector HEK 293T cells were co-transfected with S protein and a DSP_{1-7} expressing plasmid, the target cells were transfected with DSP_{8-11} plasmid. Before the target cells were transferred to the effector cells, bergamottin was added to the effector cells and incubated for 1h. The relative luminescence units were calculated and representative images were captured 24 h later (data not shown). Three independent replicates are shown. (E) Effect of bergamottin on the binding between SARS-CoV-2 RBD and ACE2. Gradient diluted bergamottin or vehicle was added to compete with ACE2-His to combine with immobilized SARS-CoV-2 S Protein RBD. The OD_{450nm} was measured using a microplate reader. Data represents mean ± SD for n = 2 biological replicates. (F) Impacts of bergamottin on ACE2 and TMPRSS2 expression. Caco-2 cells were incubated with bergamottin at indicated concentrations for 24 h. Cell lysates were then subjected to a Western Blot analysis. The experiment was repeated twice. (G) The effects of bergamottin on viral RNA synthesis. The BHK-21 cells were electroporated with SARS-CoV-2 wild-type (WT) replicon, and then treated with bergamottin or vehicle, as indicated. The relative luciferase activity was measured 24h later. Data represent mean ± SD for n = 3 biological replicates. (H) Bergamottin shows negligible inhibition of $3CL^{pro}$ protease activity. The activity of purified SARS-CoV-2 $3CL^{pro}$ enzymes was measured after adding substrates. Enzyme activity in the absence and presence of bergamottin was calculated. The data shown represent two biological replicates.

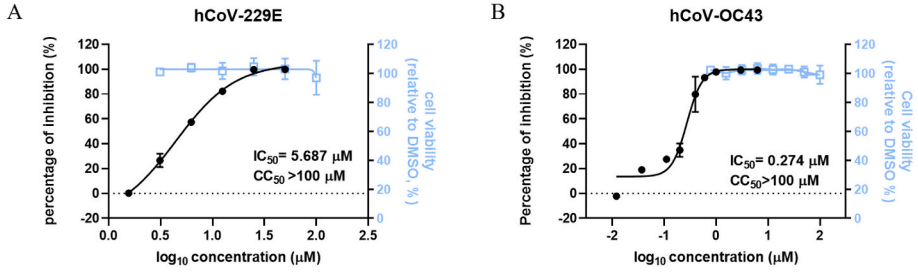

Fig. 3. Broad-spectrum antiviral effects of bergamottin on human-pathogenic coronavirus (A) Antiviral activity of bergamottin against hCoV-229E (B) Antiviral activity of bergamottin against hCoV-OC43. Viral load in the cells was quantified using RT-qPCR assays. Drug cytotoxicity was determined using a CCK-8 assay. The viral activity was measured by luciferase. Data represents mean ± SD for n = 3 biological replicates.

3.4. Antiviral activity of bergamottin in human nasal epithelial organoids

The efficacy of bergamottin against SARS-CoV-2 infection was further tested using an *ex vivo* human primary organoid model. The antiviral effect was evaluated by the reduction of viral RNA. Using remdesivir as a control (Ebisudani et al., 2021; Pei et al., 2021; Wang et al., 2021), it was found that bergamottin showed promising antiviral effects in a dose-dependent manner. When human nasal epithelial organoids were treated with 25 or 50 μM bergamottin, its inhibitory effect on SARS-CoV-2 was found to be comparable to treatment with 10 μM remdesivir, which confirmed the antiviral effect in a physiological model (Fig. 4A).

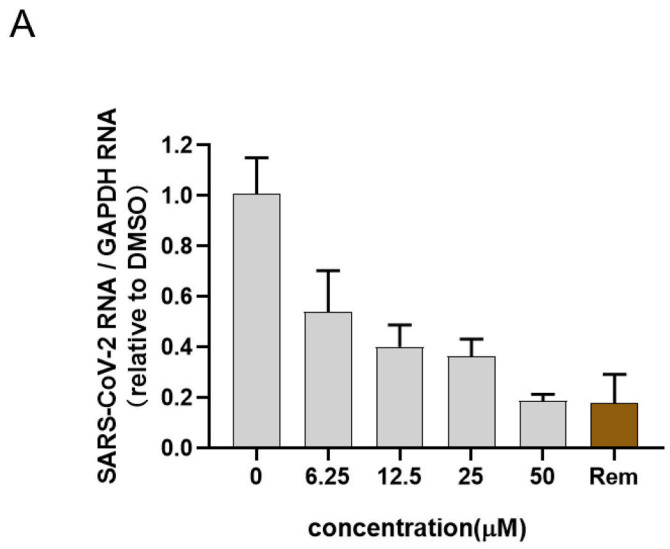

Fig. 4. Bergamottin inhibited SARS-CoV-2 infection in human epithelial nasal organoids. (A) Organoids were infected with SARS-CoV-2 in the presence of the indicated concentration of bergamottin or remdesivir as control. Viral loads in the organoids were quantified by RT-qPCR assay 24 h later. Rem represents remdesivir of 10 μM.

3.5. *In vivo* antiviral efficacy of bergamottin

As bergamottin demonstrated a robust inhibitory effect on SARS-CoV-2 infection, we sought to investigate the protective effect of bergamottin in the golden Syrian hamster model, which showed high susceptibility to infection and was a suitable animal model for the evaluation of antiviral drugs (Chan et al., 2020). The hamsters were intranasally inoculated once daily with SARS-CoV-2 (5×10^4 PFU), bergamottin, or a vehicle by gavage on 0, 1, 2, 3, and 4 days post infection (dpi) (Fig. 5A). Two dosage groups of bergamottin were administered: 50 mg/kg and 75 mg/kg. As expected, hamsters infected with SARS-CoV-2 began to appear hunch-backed, ruffled, and showed progressive weight loss over the days that followed, whereas hamsters in the bergamottin-treated group showed only slightly abnormal behavior and delayed onset of disease. Furthermore, the 75 mg/kg bergamottin group exhibited reduced weight loss caused by SARS-CoV-2 infection (Fig. 5B). With the virus proliferation peaking on day 4, hamsters were sacrificed, followed by virological and histological analyses to determine any protective effects on the viral load and histopathological changes in the nasal turbinates and lung tissues.

As shown in Fig. 5C, the administration of both 50 mg/kg and 75 mg/kg of bergamottin reduced the viral titer in nasal turbinates and lung tissues compared to the vehicle group. Likewise, the yield of viral RNA in nasal turbinates and lung tissues was reduced after bergamottin treatment, with the 75 mg/kg bergamottin dose showing a superior therapeutic effect (Fig. 5D). Histopathological analyses revealed that SARS-CoV-2 infection-induced apparent pathological damage, including alveolar structure destruction, hemorrhage, and inflammatory cell infiltration in the lung parenchyma, while bergamottin treatment mitigated these phenomena (Fig. 5E). The working concentration of bergamottin did not show any side effects in hamsters based on their daily states and weights when bergamottin was administered alone. These results suggest that bergamottin could alleviate histopathological changes and decrease viral loads in nasal turbinates and lung tissues, thereby protecting hamsters from SARS-CoV-2 infection and confirming the curative effects of bergamottin on virus-associated pneumonia.

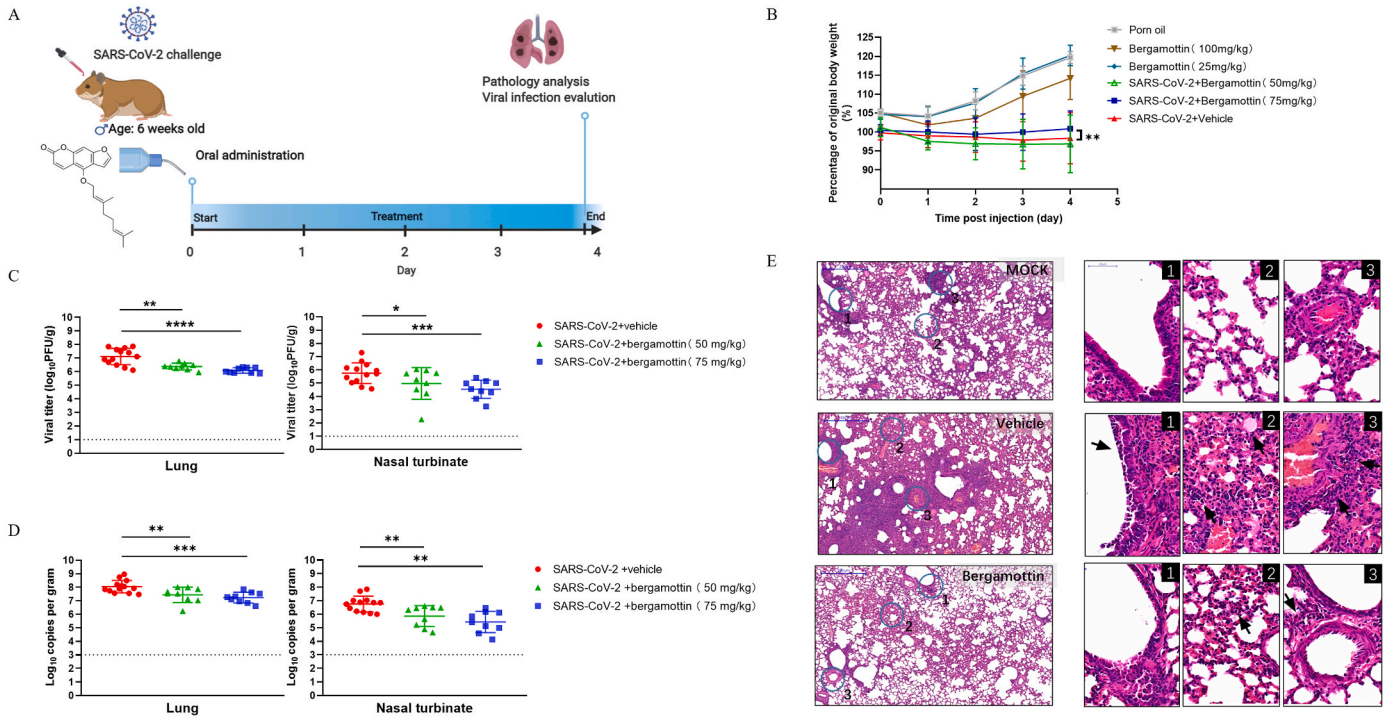

Fig. 5. Antiviral evaluation of bergamottin in the golden Syrian hamster model. (A) Experimental design of *in vivo* study: Hamsters were intranasally inoculated with 5×10^4 PFU of SARS-CoV-2, followed by virus challenge where hamsters were orally administrated 50 mg/kg (n = 9) and 75 mg/kg (n = 9) bergamottin doses for four consecutive days. The vehicle group (n = 13) was given corn oil as a control. (B) Daily body weight change curves. (C) Viral yields in the hamster lung tissues and nasal turbinates were harvested at 4 dpi and titrated by plaque assay. (D)Viral loads in the hamster lung tissues and nasal turbinates were subjected to SARS-CoV-2 viral copy detection by RT-qPCR assays. (E) Representative images of H&E-stained lung tissues section from hamsters treated with different groups as indicated. Numbered circled areas are shown in magnified images to the right, illustrating the severity of (1) Bronchiolar epithelium cell death; (2) Destruction of alveoli with massive alveolar space infiltration; (3) Intra-endothelium and perivascular infiltration. Scale bar, 500 μm. Dashed lines indicate the limit of detection. **** $P < 0.0001$; *** $P < 0.001$; ** $P < 0.01$; * $P < 0.05$.

4. Discussion

We provided evidence that bergamottin is effective against SARS-CoV-2 and emerging variants at micromolar non-toxic concentrations with a high selective index in human cell lines. Bergamottin demonstrated significant dose-dependent inhibition of SARS-CoV-2 in human nasal epithelial organoids, an *ex vivo* preclinical model derived directly from patient samples, which robustly supported SARS-CoV-2 infection. (Liu et al., 2020; Rajan et al., 2022). The optimal protective effect of bergamottin on SARS-CoV-2 was also confirmed in the golden Syrian hamster model. Orally delivered bergamottin reduced viral loads in the nasal turbinates and lung tissues in SARS-CoV-2 infected hamsters significantly. Pneumonia and histopathological damage caused by SARS-CoV-2 infection were mitigated as well.

It was found that bergamottin interfered with multiple steps of the life cycle of the virus by blocking SARS-CoV-2 viral entry into host cells, specifically by inhibiting spike-mediated membrane fusion and inhibiting human angiotensin-converting enzyme 2 (hACE2) expression. When infection of a host cell is initiated, the virus first binds to the receptor at the receptor-binding domain located in the S1 subunit, which induces conformational changes in the S1 subunit and exposes the S2′ cleavage site in the S2 subunit. There are two distinct entry pathways following ACE2 engagement. S2 is cleaved by TMPRSS2 or cathepsin L, which mediate the cytoplasm or endosomal membrane fusion, respectively. (Jackson et al., 2022; Li, 2016; Melikyan, 2014). The result of bergamottin inhibiting membrane fusion might be due to the suppression of the cellular expression of ACE2 by bergamottin. However, it is significant to note that bergamottin, cannot block the binding interface of ACE2 to the S protein completely.

Bergamottin also inhibited the post-entry step of SARS-CoV-2 and viral replication in this study. Bergapten, an analogue of bergamottin, inhibits severe acute respiratory syndrome virus (SARS-CoV) $3CL^{pro}$ activity at 200 μM based on a cell-free trans-cleavage experiment (Park et al., 2016). However, bergamottin did not affect $3CL^{pro}$ as bergapten did, which suggested that bergamottin inhibited replication of SARS-CoV-2 through a different mechanism or pathway.

According to previous studies, bergamottin has been used to treat various malignancies *in vitro* and *in vivo*, including gastric cancer (Sekiguchi et al., 2008), fibrosarcoma (Hwang et al., 2010), and glioma (Luo et al., 2018). In the treatment of lung adenocarcinoma, intraperitoneal injection of 100 mg/kg bergamottin for 18 consecutive days, showed good antitumor activity in nude mice (Wu et al., 2016). In these experiments, bergamottin showed good biocompatibility. We found that bergamottin administration at 50 mg/kg and 75 mg/kg safely and effectively protected hamsters from SARS-CoV-2 infection, reduced SARS-CoV-2 viral loads in the nasal turbinates and lung tissues, and delayed the onset or progression of the disease. Administration of a higher dose of bergamottin resulted in better antiviral effects, indicating that bergamottin has broad potential clinical application prospects.

Currently, remdesivir, which remains the main treatment option approved by the FDA for COVID-19, shows limited effectiveness, especially in patients with severe disease (Wang et al., 2020). Additionally, its bioavailability is restricted and it can only be delivered intravenously. Most recently, the US FDA issued an emergency use authorization for Paxlovid (2022), in which nirmatrelvir and ritonavir acted as an active $3CL^{pro}$ inhibitor and a pharmacokinetic enhancer, respectively, by inhibiting the activity of hepatic cytochrome P450 3A4 (CYP450) isoenzyme. Doses of 100 mg ritonavir and 300 mg nirmatrelvir administered to adults twice a day for 5 days seemed an ingenious drug combination regimen (Wen et al., 2022).

Our results suggest that bergamottin, a widely available natural furanocoumarin, could be a potential inhibitor of SARS-CoV-2. Notably, bergamottin is known to inhibit CYP450 activity as ritonavir does, which could potentially be used in combination with other drugs to improve the efficacy of the antiviral effect, shedding new light on drug combinations with bergamottin and other substrate drugs.

Author contributions

W.W. had the concept, devised the study, made critical revisions of the manuscript for important intellectual content, and made supervision. W.W. and G.X. provided the funding support for the project. M.Z. performed most of the experiments, and participate in data curation, investigation, visualization, and original raft writing. J.C., Y.L. contributed to developing methodology, investigation, validation, and formal analysis. G.L., Y.Y., B.Z., kindly provided materials support and resources. Y.H., D. Q, Y.Z. Q.Z. help to perform experiments investigation and formal analysis.

Declaration of competing interest

There are no competing interests to declare.

Acknowledgments

We thank Tao Du, Jin Xiong, Jia Wu, Jun Liu, and Hao Tang from the BSL-3 Laboratory of the Wuhan Institute of Virology for their critical support. We thank the Institutional Center for Shared Technologies and Facilities; Center for Instrumental Analysis and Metrology of Wuhan Institute of Virology, CAS, for providing technical assistance. This work was supported by the National Key Research and Development Program of China (2018YFA0507204), the National Natural Science Foundation of China of China (82172273, 31670165), Wuhan National Biosafety Laboratory, Chinese Academy of Sciences Advanced Customer Cultivation Project (2019ACCP-MS03), the Open Research Fund Program of the State Key Laboratory of Virology of China (2018IOV001).

References

Acciani, M., Alston, J.T., Zhao, G., Reynolds, H., Ali, A.M., Xu, B., Brindley, M.A., 2017. Mutational analysis of Lassa virus glycoprotein highlights regions required for alpha-dystroglycan utilization. J. Virol. 91.

Awadasseid, A., Wu, Y., Tanaka, Y., Zhang, W., 2021. Current advances in the development of SARS-CoV-2 vaccines. Int. J. Biol. Sci. 17, 8–19.

Benton, D.J., Wrobel, A.G., Xu, P., Roustan, C., Martin, S.R., Rosenthal, P.B., Skehel, J.J., Gamblin, S.J., 2020. Receptor binding and priming of the spike protein of SARS-CoV-2 for membrane fusion. Nature 588, 327–330.

Cao, J., Liu, Y., Zhou, M., Dong, S., Hou, Y., Jia, X., Lan, X., Zhang, Y., Guo, J., Xiao, G., Wang, W., 2022. Screening of botanical drugs against SARS-CoV-2 entry reveals novel therapeutic agents to treat COVID-19. Viruses 14, 353.

Chan, J.F., Zhang, A.J., Yuan, S., Poon, V.K., Chan, C.C., Lee, A.C., Chan, W.M., Fan, Z., Tsoi, H.W., Wen, L., Liang, R., Cao, J., Chen, Y., Tang, K., Luo, C., Cai, J.P., Kok, K. H., Chu, H., Chan, K.H., Sridhar, S., Chen, Z., Chen, H., To, K.K., Yuen, K.Y., 2020. Simulation of the clinical and pathological manifestations of coronavirus disease 2019 (COVID-19) in a golden Syrian hamster model: implications for disease pathogenesis and transmissibility. Clin. Infect. Dis. 71, 2428–2446.

Choi, H.J., Lim, C.H., Song, J.H., Baek, S.H., Kwon, D.H., 2009. Antiviral activity of raoulic acid from Raoulia australis against Picornaviruses. Phytomedicine 16, 35–39.

Ebisudani, T., Sugimoto, S., Haga, K., Mitsuishi, A., Takai-Todaka, R., Fujii, M., Toshimitsu, K., Hamamoto, J., Sugihara, K., Hishida, T., Asamura, H., Fukunaga, K., Yasuda, H., Katayama, K., Sato, T., 2021. Direct derivation of human alveolospheres for SARS-CoV-2 infection modeling and drug screening. Cell Rep. 35, 109218.

Hu, B., Guo, H., Zhou, P., Shi, Z.L., 2021. Characteristics of SARS-CoV-2 and COVID-19. Nat. Rev. Microbiol. 19, 141–154.

Hwang, Y.P., Yun, H.J., Choi, J.H., Kang, K.W., Jeong, H.G., 2010. Suppression of phorbol-12-myristate-13-acetate-induced tumor cell invasion by bergamottin via the inhibition of protein kinase Cdelta/p38 mitogen-activated protein kinase and JNK/nuclear factor-kappaB-dependent matrix metalloproteinase-9 expression. Mol. Nutr. Food Res. 54, 977–990.

Jackson, C.B., Farzan, M., Chen, B., Choe, H., 2022. Mechanisms of SARS-CoV-2 entry into cells. Nat. Rev. Mol. Cell Biol. 23, 3–20.

Lan, J., Ge, J., Yu, J., Shan, S., Zhou, H., Fan, S., Zhang, Q., Shi, X., Wang, Q., Zhang, L., Wang, X., 2020. Structure of the SARS-CoV-2 spike receptor-binding domain bound to the ACE2 receptor. Nature 581, 215–220.

Li, F., 2016. Structure, function, and evolution of coronavirus spike proteins. Ann. Rev. Virol. 3, 237–261.

Lin, L.T., Chen, T.Y., Lin, S.C., Chung, C.Y., Lin, T.C., Wang, G.H., Anderson, R., Lin, C.C., Richardson, C.D., 2013. Broad-spectrum antiviral activity of chebulagic acid and punicalagin against viruses that use glycosaminoglycans for entry. BMC Microbiol. 13, 187.

Lin, L.T., Hsu, W.C., Lin, C.C., 2014. Antiviral natural products and herbal medicines. J. Tradit. Complement. Med. 4, 24–35.

Liu, Z., Anderson, J.D., Deng, L., Mackay, S., Bailey, J., Kersh, L., Rowe, S.M., Guimbellot, J.S., 2020. Human nasal epithelial organoids for therapeutic development in cystic fibrosis. Genes 11.
Liu, Y., Guo, J., Cao, J.Y., Zhang, G.S., Jia, X.Y., Wang, P.L., Xiao, G.F., Wang, W., 2021. Screening of botanical drugs against Lassa virus entry. J. Virol. 95.
Luo, W., Song, Z., Sun, H., Liang, J., Zhao, S., 2018. Bergamottin, a natural furanocoumarin abundantly present in grapefruit juice, suppresses the invasiveness of human glioma cells via inactivation of Rac1 signaling. Oncol. Lett. 15, 3259–3266.
Melikyan, G.B., 2014. HIV entry: a game of hide-and-fuse? Curr. Opin. Virol. 4, 1–7.
Park, J.Y., Ko, J.A., Kim, D.W., Kim, Y.M., Kwon, H.J., Jeong, H.J., Kim, C.Y., Park, K.H., Lee, W.S., Ryu, Y.B., 2016. Chalcones isolated from Angelica keiskei inhibit cysteine proteases of SARS-CoV. J. Enzym. Inhib. Med. Chem. 31, 23–30.
Paxlovid for treatment of COVID-19. Med. Lett. Drugs Ther. 64, 9-10.
Pei, R., Feng, J., Zhang, Y., Sun, H., Li, L., Yang, X., He, J., Xiao, S., Xiong, J., Lin, Y., Wen, K., Zhou, H., Chen, J., Rong, Z., Chen, X., 2021. Host metabolism dysregulation and cell tropism identification in human airway and alveolar organoids upon SARS-CoV-2 infection. Protein Cell 12, 717–733.
Rajan, A., Weaver, A.M., Aloisio, G.M., Jelinski, J., Johnson, H.L., Venable, S.F., McBride, T., Aideyan, L., Piedra, F.A., Ye, X., Melicoff-Portillo, E., Yerramilli, M.R.K., Zeng, X.L., Mancini, M.A., Stossi, F., Maresso, A.W., Kotkar, S.A., Estes, M.K., Blutt, S., Avadhanula, V., Piedra, P.A., 2022. The Human Nose Organoid Respiratory Virus Model: an Ex Vivo Human Challenge Model to Study Respiratory Syncytial Virus (RSV) and Severe Acute Respiratory Syndrome Coronavirus 2 (SARS-CoV-2) Pathogenesis and Evaluate Therapeutics. mBio, e0351121.
Sekiguchi, H., Washida, K., Murakami, A., 2008. Suppressive effects of selected food phytochemicals on CD74 expression in NCI-N87 gastric carcinoma cells. J. Clin. Biochem. Nutr. 43, 109–117.
V'Kovski, P., Kratzel, A., Steiner, S., Stalder, H., Thiel, V., 2021. Coronavirus biology and replication: implications for SARS-CoV-2. Nat. Rev. Microbiol. 19, 155–170.
Vijgen, L., Keyaerts, E., Moes, E., Maes, P., Duson, G., Van Ranst, M., 2005. Development of one-step, real-time, quantitative reverse transcriptase PCR assays for absolute quantitation of human coronaviruses OC43 and 229E. J. Clin. Microbiol. 43, 5452–5456.
Wang, C., Horby, P.W., Hayden, F.G., Gao, G.F., 2020. A novel coronavirus outbreak of global health concern. Lancet 395, 470–473.
Wang, C., Zhang, M., Garcia Jr., G., Tian, E., Cui, Q., Chen, X., Sun, G., Wang, J., Arumugaswami, V., Shi, Y., 2021. ApoE-isoform-dependent SARS-CoV-2 neurotropism and cellular response. Cell Stem Cell 28, 331–342 e335.
Wen, W., Chen, C., Tang, J., Wang, C., Zhou, M., Cheng, Y., Zhou, X., Wu, Q., Zhang, X., Feng, Z., Wang, M., Mao, Q., 2022. Efficacy and safety of three new oral antiviral treatment (molnupiravir, fluvoxamine and Paxlovid) for COVID-19a meta-analysis. Ann. Med. 54, 516–523.
Wu, H.J., Wu, H.B., Zhao, Y.Q., Chen, L.J., Zou, H.Z., 2016. Bergamottin isolated from Citrus bergamia exerts in vitro and in vivo antitumor activity in lung adenocarcinoma through the induction of apoptosis, cell cycle arrest, mitochondrial membrane potential loss and inhibition of cell migration and invasion. Oncol. Rep. 36, 324–332.
Yu, S., Zheng, X., Zhou, B., Li, J., Chen, M., Deng, R., Wong, G., Lavillette, D., Meng, G., 2022. SARS-CoV-2 spike engagement of ACE2 primes S2' site cleavage and fusion initiation. Proc. Natl. Acad. Sci. U. S. A. 119.
Zandi, K., Teoh, B.T., Sam, S.S., Wong, P.F., Mustafa, M.R., Abubakar, S., 2012. Novel. Antiviral activity of baicalein against dengue virus. BMC Compl. Alternative Med. 12, 214.
Zhang, Q.Y., Deng, C.L., Liu, J., Li, J.Q., Zhang, H.Q., Li, N., Zhang, Y.N., Li, X.D., Zhang, B., Xu, Y., Ye, H.Q., 2021. SARS-CoV-2 replicon for high-throughput antiviral screening. J. Gen. Virol. 102.
Zhou, P., Yang, X.L., Wang, X.G., Hu, B., Zhang, L., Zhang, W., Si, H.R., Zhu, Y., Li, B., Huang, C.L., Chen, H.D., Chen, J., Luo, Y., Guo, H., Jiang, R.D., Liu, M.Q., Chen, Y., Shen, X.R., Wang, X., Zheng, X.S., Zhao, K., Chen, Q.J., Deng, F., Liu, L.L., Yan, B., Zhan, F.X., Wang, Y.Y., Xiao, G.F., Shi, Z.L., 2020. A pneumonia outbreak associated with a new coronavirus of probable bat origin. Nature 579, 270–273.
Zhu, Y., Yu, D., Yan, H., Chong, H., He, Y., 2020. Design of potent membrane fusion inhibitors against SARS-CoV-2, an emerging coronavirus with high fusogenic activity. J. Virol. 94.